Note on the Rayleigh waves properties in viscoelastic media

J. Y. LE POMMELLEC, A. EL BAROUDI[*]

Arts et Metiers Institute of Technology, 2 boulevard du Ronceray,
49035 Angers, France, e-mail[*]: adil.elbaroudi@ensam.eu (corresponding author)

THIS PAPER DESCRIBES A THEORY for surface Rayleigh waves propagating in a viscoelastic medium. The Zener model to describe the viscoelastic behavior of the medium is used. This simple model captures both the relaxation and retardation. An analytical expression for the complex dispersion equation of Rayleigh waves is established. The influence of the normalized frequency and the ratio of shear moduli on the dispersion curves of the Rayleigh wave velocity and attenuation is analyzed numerically. The numerical solutions show the dependence of the phase velocity change and the wave attenuation in terms of the normalized frequency and the ratio of shear moduli. As an important result, the Zener model can be used at a normalized low frequency to predict creep phenomenon as well as at a normalized high frequency to predict relaxation. The obtained results are fundamental and can be applied to characterize the viscoelastic properties of soft biomaterials and tissue, in nondestructive testing of materials, in geophysics and seismology. Thus, the obtained complex dispersion equation can be very useful to interpret the experimental measurements of Rayleigh waves propertie in a viscoelastic medium.

Key words: Rayleigh waves, viscoelastic materials, Zener model, analytical resolution.

1. Introduction

VISCOELASTIC MATERIALS ARE WIDELY USED IN INDUSTRY, especially, polymers in automobile and aeronautics industries as well as in the medical field. The macroscopic description of these materials includes both fluid-like and solid-like characteristics. During mechanical tests (creep or relaxation), the response depends on time (or frequency during dynamic experiments). This behavior is modeled by the combination of springs and dashpots in series or in parallel [1, 2]. Therefore, different rheological models are used to describe linear viscoelasticity. Thus, common two-element rheological models include the Maxwell and Kelvin–Voigt models. More precisely, the Maxwell model consists of a Hookean spring in series with a Newtonian dashpot while in the Kelvin–Voigt model the spring and the dashpot are parallel. Notably, the Maxwell

model is adapted to viscoelastic liquid while the Kelvin–Voigt model describes viscoelastic solids. However, the Kelvin–Voigt model used in References [3–7] can only predict the creep behavior and is not sufficient to model viscoelastic polymers [8, 9]. It is therefore necessary to improve the Kelvin–Voigt model. Thus, models with three elements were developed to more realistically characterize the creep recovery and stress relaxation behavior of a viscoelastic polymer. These models include the standard linear solid model, also known as the Zener model [10–12], which consists of two Hookean springs and one Newtonian dashpot.

The rheological models above described are useful to develop characterization methods of materials viscoelasticity [3, 6, 7]. In particular, the soft tissue viscoelastic properties provide information about their pathological condition [13–19]. Furthermore, the knowledge of viscoelastic properties of biomaterials such as hydrogel is very important in the field of tissue engineering [20–24]. There is also a growing demand for surface acoustic wave sensors (Love and Rayleigh) intended to control the viscoelastic properties of materials. Especially, the Rayleigh waves travel near the surface of solids and include both longitudinal and transverse motions [25–28]. The depth of significant displacement in the solid is approximately equal to the acoustic wavelength. Moreover, the Rayleigh waves propagation velocity is smaller than that of the volume wave. Due to these properties, the Rayleigh waves have considerable applications. Particularly, the propagation of Rayleigh waves in thermoelastic materials has numerous applications in various fields of science and technology [29–31]. In the field of quality control, these waves are widely used for the non-destructive measurement and evaluation of surface cracks [32, 33]. In geophysics Rayleigh waves diffraction are used for the detection of near surface features such as voids and faults [34–39]. In medicine, the Rayleigh waves are also the subject of great interest. Indeed, the Rayleigh waves make it possible to characterize a viscoelastic soft biological tissues in a non invasive manner [40–45].

In this paper, an analytical approach based on the Zener model is proposed to predict the phase velocity and the attenuation coefficient of the Rayleigh wave. This wave propagating in such viscoelastic media undergo attenuation, hence, the Rayleigh wavenumber becomes complex. The real part of this wavenumber determines the phase velocity and its imaginary part represents the attenuation coefficient. In other word, the complex wavenumber includes information about both the propagation and dissipation of the Rayleigh wave at different frequencies. The frequency-dependent complex wavenumber was calculated using a dispersion relation established analytically in this paper. The results obtained are fundamental and can be very useful to interpret the experimental measurements of Rayleigh waves properties in viscoelastic media.

1.1. Viscoelastic constitutive equation

The use of mechanical models to describe the materials behavior is well known [10, 46–48]. Most polymers do not exhibit viscoelastic behavior described by the simple Maxwell and Kelvin models because the conformational changes and the viscous flow are constrained by a multitude of physical entanglements and chemical crosslinks which impair viscoelastic flow in a very complicated way. The situation is further complicated if the polymer in question has a complex morphology such as crystalline domains dispersed in an amorphous matrix, microphase separated polymer domains and interpenetrated polymer networks. For these materials, more elaborate spring dashpot models have to be employed to effectively describe their complicated viscoelastic behavior.

The model that captures both the relaxation and retardation is known as the three-parameter model. This model is obtained by adding a spring either in series to the Kelvin–Voigt model or in parallel to the Maxwell model. This model is sometimes referred to as the Zener Model and is employed to describe a material that will fully recover after a load is removed because the spring connected in parallel to the Maxwell element will continue to move the piston of the dashpot back to its original position. Therefore, the simplest approach to describe viscoelasticity assumes that the material consists of a viscous element and two elastic components. Thus, the constitutive equation describes the relation between force and deformation is expressed in the following form [49]:

$$(1.1) \qquad G_1 \boldsymbol{\tau} + \eta \frac{\partial \boldsymbol{\tau}}{\partial t} = 2 G_1 G_2 \boldsymbol{\varepsilon} + 2(G_1 + G_2) \eta \frac{\partial \boldsymbol{\varepsilon}}{\partial t},$$

where η is the viscosity, G is the shear modulus, and $\boldsymbol{\varepsilon}$ stands for the strain tensor. Qualitatively, this model describes the behavior of a typical polymer. The Kelvin–Voigt model gives retarded elastic behavior and represents a crosslinked polymer. The Maxwell model gives steady-state creep and represents an uncrosslinked polymer. With an appropriate choice of G_1 and G_2, the Zener model can describe both types of behavior. A temporal Fourier transform, convention $f(\omega) = \int f(t) e^{j\omega t} \, dt$, readily relates the dynamic shear stress $\boldsymbol{\tau}(\omega) = 2G(\omega)\boldsymbol{\varepsilon}(\omega)$ linearly to the dynamic strain $\boldsymbol{\varepsilon}(\omega)$, where $G(\omega)$ is known as the complex elastic modulus. Explicitly, for the Zener model one finds:

$$(1.2) \qquad \frac{G(\omega)}{G_1} = \alpha - \frac{j\omega\delta}{1 - j\omega\delta},$$

where the Zener time $\delta = \eta/G_1$ characterizes the crossover from elastic to viscous behavior, and $\alpha = G_2/G_1$ represents the ratio of the shear moduli. Note that the real part of the complex elastic modulus refers to the storage modulus and its imaginary part to the loss modulus [8, 9]. Since the Zener model is connected

by a spring in parallel with the Maxwell model, we can deduce the complex shear modulus for Maxwell and Kelvin–Voigt models as below:

(1.3) $$\frac{G(\omega)}{G_1} = -\frac{j\omega\delta}{1 - j\omega\delta}, \quad \text{for Maxwell model,}$$

(1.4) $$\frac{G(\omega)}{G_1} = 1 - j\omega\delta, \quad \text{for Kelvin–Voigt model.}$$

Figure 1 shows the complex shear modulus for such a Zener solid. For frequencies $\omega\delta < 1$, the loss modulus for $\alpha = 0$ (i.e. Maxwell) dominates over the storage modulus indicative of viscous behavior. However, when the storage modulus dominates over the loss modulus indicative of elastic behavior. For $\alpha \neq 0$ two plateaus are highlighted for $\delta\omega \ll 1$ and $\delta\omega \gg 1$. For $\delta\omega \ll 1$ the behavior of the Zener model is analogous to that of Kelvin–Voigt (creep). For $\delta\omega \gg 1$ the behavior of the Zener model is analogous to that of Maxwell (relaxation). Between these two limits the behavior is viscoelastic. For $\alpha = 0.1$ a very important behavior can be highlighted. For $\delta\omega \leq 0.1$ the behavior is viscoelastic with a dominant elastic component. For $0.1 \leq \delta\omega \leq 0.8$ the behavior is viscoelastic with a dominant viscous component. For $\delta\omega \geq 0.8$ the behavior is viscoelastic with a dominant elastic component before reaching the elastic plateau. For any $\alpha > 0.2$ the behavior between the two limits is viscoelastic with a dominant elastic component.
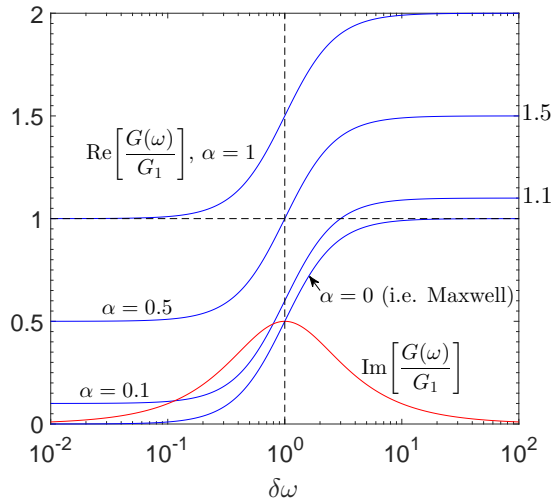
Fig. 1. Real (blue curve) and imaginary (red curve) part of the complex shear modulus as a function of normalized frequency $\omega\delta$ for a Zener model for different values of α.

2. Rayleigh wave propagation in viscoelastic media

Rayleigh waves are surface waves which are confined near stress-free boundaries in half spaces. They involve interactions between compressional and shear waves [25]. Rayleigh waves include motion in both the longitudinal and transverse directions, in particular a two-dimensional rolling motion along the xz plane. The amplitude of the propagating surface wave decreases as z increases in the half space. In this paper, the half space is assumed to be viscoelastic. Therefore, the wave amplitude decreases as x increases because of dissipation in the viscoelastic half space. The momentum conservation's equation governs the wave motion in the medium. In the absence of body forces, the equation is written in the form:

$$(2.1) \qquad \rho \frac{\partial^2 \mathbf{u}}{\partial t^2} = \nabla \cdot \boldsymbol{\sigma},$$

in which ρ is the material density and $\mathbf{u}$ is the displacement vector, is the stress tensor. The total stress in viscoelastic media, $\boldsymbol{\sigma}$, can be written as:

$$(2.2) \qquad \boldsymbol{\sigma} = \lambda (\nabla \cdot \mathbf{u}) \mathbf{I} + \boldsymbol{\tau},$$

where λ is the Lamé's first parameter, $\mathbf{I}$ is the identity tensor and the shear stress tensor $\boldsymbol{\tau}$ satisfies the constitutive equation (1.1). In order to obtain a generalized form of momentum equation for viscoelastic media, we start by applying the divergence operator to both sides of above equation and taking into account Eqs. (1.2) and (2.1), yields the following generalized unsteady momentum equation for the viscoelastic media as:

$$(2.3) \qquad \frac{\rho}{G_1} \left(\frac{\partial^2 \mathbf{u}}{\partial t^2} + \delta \frac{\partial^3 \mathbf{u}}{\partial t^3} \right) = \left[\frac{\lambda}{G_1} + \alpha + \delta \left(1 + \alpha + \frac{\lambda}{G_1} \right) \frac{\partial}{\partial t} \right] \nabla \nabla \cdot \mathbf{u}$$
$$+ \left[\alpha + \delta(1 + \alpha) \frac{\partial}{\partial t} \right] \nabla^2 \mathbf{u}.$$

It is easily seen from the above equation that the elastic theory is recovered when the Zener time parameter δ is set identically to zero (i.e. $\eta = 0$). Thus, Eq. (2.3) becomes Navier's equation as follow [25]:

$$\rho \frac{\partial^2 \mathbf{u}}{\partial t^2} = G_2 \nabla^2 \mathbf{u} + (\lambda + G_2) \nabla \nabla \cdot \mathbf{u}.$$

Therefore, any sufficiently smooth vector field can be written in terms of the sum of the gradient of a scalar potential and the curl of a vector potential. This is called the Helmholtz representation [50]. For the displacement field considered here, that representation is:

$$(2.4) \qquad \mathbf{u} = \nabla \phi + \nabla \times \boldsymbol{\psi}$$

with the Gauge condition $\nabla \cdot \boldsymbol{\psi} = 0$, and $\boldsymbol{\psi} = (0, \psi, 0)$ due to the two-dimensional nature of the problem. Thus, ϕ and ψ are the compressional and shear wave potentials. Substitution of the above equation into the equation of motion (2.3), after some manipulations, yields:

$$(2.5) \quad \left\{ \frac{\lambda}{G_1}\left(1 + \delta\frac{\partial}{\partial t}\right) + 2\left[\alpha + \delta(1 + \alpha)\frac{\partial}{\partial t}\right] \right\} \nabla^2 \phi - \frac{\rho}{G_1}\left(1 + \delta\frac{\partial}{\partial t}\right)\frac{\partial^2 \phi}{\partial t^2} = 0,$$

$$(2.6) \quad \left[\alpha + \delta(1 + \alpha)\frac{\partial}{\partial t}\right]\nabla^2 \psi - \frac{\rho}{G_1}\left(1 + \delta\frac{\partial}{\partial t}\right)\frac{\partial^2 \psi}{\partial t^2} = 0.$$

The determination of the scalar potentials ϕ and ψ requires the resolution of the above equations; if the harmonic motion is considered as $f(\mathbf{x}, t) = f(\mathbf{x})e^{-j\omega t}$, ϕ and ψ take the following forms:

$$(2.7) \qquad \phi = Ae^{-\beta_c z}e^{j(kx - \omega t)},$$

$$(2.8) \qquad \psi = Be^{-\beta_s z}e^{j(kx - \omega t)},$$

in which $k = k_r + jk_i$ is the complex Rayleigh wavenumber along the propagation direction, A and B are the unknown amplitudes of the corresponding potentials and:

$$(2.9) \qquad \beta_c^2 = k^2 - k_c^2, \qquad \beta_s^2 = k^2 - k_s^2,$$

where the complex wavenumbers k_c and k_s are expressed as:

$$(2.10) \qquad k_c = \frac{\omega}{c_c}, \qquad k_s = \frac{\omega}{c_s},$$

where c_c and c_s are the complex compressional and shear wave velocities in the medium, respectively; and are expressed as:

$$(2.11) \qquad c_c = \sqrt{\frac{\lambda(\omega) + 2G(\omega)}{\rho}}, \qquad c_s = \sqrt{\frac{G(\omega)}{\rho}},$$

in which $G(\omega)$ is the complex shear modulus given in Eq. (1.2). Therefore, since the motion is harmonic the stress tensor may be written as:

$$(2.12) \qquad \boldsymbol{\sigma} = \lambda(\omega)(\nabla \cdot \mathbf{u})\mathbf{I} + 2G(\omega)\boldsymbol{\varepsilon}$$

and the complex, frequency-dependent Lamé's first parameter is determined according to the relation:

$$(2.13) \qquad \lambda(\omega) = \frac{2\nu}{1 - 2\nu}G(\omega),$$

where ν is the Poisson ratio of the medium. Considering the fundamental field equations in a Cartesian coordinate system and using the Helmholtz decomposition given in Eq. (2.14), the displacement components for the Rayleigh wave are defined as:

$$(2.14) \qquad u_x = [jkAe^{-\beta_c z} + \beta_s Be^{-\beta_s z}]e^{j(kx-\omega t)},$$

$$(2.15) \qquad u_z = [jkBe^{-\beta_s z} - \beta_c Ae^{-\beta_c z}]e^{j(kx-\omega t)}.$$

Also, according to the generalized constitutive Eq. (2.12), the relevant stress components that will further used in boundary conditions are given by:

$$(2.16) \qquad \sigma_{zz} = -G(\omega)[2jk\beta_c Ae^{-\beta_c z} + (\beta_s^2 + k^2)Be^{-\beta_s z}]e^{j(kx-\omega t)},$$

$$(2.17) \qquad \sigma_{xz} = -G(\omega)[2jk\beta_s Be^{-\beta_s z} - (\beta_s^2 + k^2)Ae^{-\beta_c z}]e^{j(kx-\omega t)}.$$

The complex dispersion equation for the propagating Rayleigh waves shall be obtained by application of the appropriate boundary conditions. Therefore, the specific boundary conditions that need to be satisfied on the stress-free boundary (i.e., at $z = 0$) are $\sigma_{xz} = 0$ and $\sigma_{zz} = 0$. Consequently, utilization of the stress relations in the boundary conditions yields the following dissipation equation, ensuring nontrivial solutions for A and B:

$$(2.18) \qquad \left(2 - \frac{k_s^2}{k^2}\right)^4 - 16\left(1 - \frac{k_s^2}{k^2}\right)\left(1 - \frac{1-2\nu}{2-2\nu}\frac{k_s^2}{k^2}\right) = 0.$$

Since Eq. (2.18) contains k, ω, as well as all material parameters of the viscoelastic medium, Eq. (2.18) represents the implicit complex dispersion equation of Rayleigh waves propagating in a semi infinite viscoelastic medium. Equation (2.18) was solved using Mathematica software. Once the wavenumber is obtained, the Rayleigh wave velocity can be calculated by $v = \omega/k_r$. While the imaginary part of wavenumber k_i represents the attenuation per unit length in the propagation direction. Note that the dispersion equation of the Rayleigh wave in an elastic medium is obtained by replacing k_s in Eq. (2.18) by $k_t = \omega/c_t$, where $c_t = \sqrt{G_1/\rho}$ represents the shear wave velocity in the solid.

3. Numerical results and discussion

In order to plot the behavior of the complex Rayleigh wavenumber, the material properties used in this paper are $G_1/\rho = 230\,\mathrm{m}^2 \cdot \mathrm{s}^{-2}$ and $\nu = 0.4$, and similar to those used by CATHELINE *et al.* [3].

3.1. Rayleigh wavenumber for for Maxwell and Kelvin–Voigt models

In this section we investigate the effect of the normalized frequency $\omega\delta$ on the Rayleigh wavenumber for Maxwell and Kelvin–Voigt models. The frequency used for the numerical calculations is equal to $100\,\mathrm{Hz}$. Therefore, the normalized frequency becomes $\delta\omega = 200\pi\delta$. In particular, the curves are obtained by varying the Zener time, i.e. δ. In this case, the wavenumber characterizing the elastic medium k_t does not depend on the angular frequency ω. Otherwise, $k_t = 200\pi/c_t$ has a constant value equal to $41.43\,\mathrm{m}^{-1}$. It can be seen from Fig. 2 that the real part of the Rayleigh wavenumber for the Maxwell model $k_r^{(\mathrm{m})}$ decreases with $\omega\delta$ and reaches a plateau region for $\omega\delta \geq 1$. Otherwise, its imaginary part $k_i^{(\mathrm{m})}$ decreases monotonically with $\omega\delta$. Possible physical explanation for this asymptotic behavior may be that the Rayleigh wave is similar to a shear wave (i.e. the compression term $\nabla\nabla \cdot \mathbf{u}$ in Eq. (2.3) is negligible). In order to obtain the asymptotic values, a one-dimensional (i.e. $\beta_s = 0$) shear wave is considered. Using the first-order Taylor polynomial of the real and imaginary parts of the wavenumber $k = k_s$, the following asymptotic relations are obtained:

$$
(3.1) \quad
\begin{aligned}
k_r^{(\mathrm{m})} &= k_i^{(\mathrm{m})} = \frac{k_t}{\sqrt{\delta\omega}} \quad \text{for } \delta\omega \ll 1, \\
k_r^{(\mathrm{m})} &= k_t, \quad k_i^{(\mathrm{m})} = \frac{k_t}{\sqrt{2\delta\omega}} \quad \text{for } \delta\omega \gg 1.
\end{aligned}
$$

These analytical expressions are very consistent with the curves obtained with the dispersion equation (2.18). Moreover, Fig. 2 also shows that for the Maxwell model the medium behaviors are respectively viscous and elastic for $\delta\omega \ll 1$ and $\delta\omega \gg 1$. Between these two limits the medium acts like viscoelastic.

The opposite phenomenon appears for the Kelvin–Voigt model. The real part of the Rayleigh wavenumber $k_r^{(\mathrm{kv})}$ keeps a constant value and begins to drop for $\omega\delta \geq 0.5$. Besides, its imaginary part $k_i^{(\mathrm{kv})}$ increases with $\omega\delta$, attains a maximum value for $\omega\delta = 1$ and then falls off. It is seen that the real and imaginary parts of the Rayleigh wavenumber join for $\omega\delta \geq 10$. These curves are coherent with asymptotic relations given below:

$$
(3.2) \quad
\begin{aligned}
k_r^{(\mathrm{kv})} &= k_t, \quad k_i^{(\mathrm{kv})} = \frac{k_t\delta\omega}{\sqrt{2}} \quad \text{for } \delta\omega \ll 1, \\
k_r^{(\mathrm{kv})} &= k_i = \frac{k_t}{\sqrt{\delta\omega}} \quad \text{for } \delta\omega \gg 1.
\end{aligned}
$$

Similarly, these asymptotic relations are obtained using the first-order Taylor polynomial. In addition, Fig. 2 illustrates that for the Kelvin–Voigt model the medium behaviors are respectively viscous and elastic for $\delta\omega \gg 1$ and $\delta\omega \ll 1$. Between these two limits the medium acts like viscoelastic.

Figure 2 provides the influence of the normalized frequency $\delta\omega$ on the ratio k_r/k_i for Maxwell and Kelvin–Voigt models. We notice that this ratio increases with d for Maxwell model and decreases in the case of Kelvin–Voigt model. Otherwise, we remark that this ratio converges to 1 when $\delta\omega \ll 1$ for the Maxwell model and when $\delta\omega \gg 1$ for the Kelvin–Voigt model. This reveals the viscous character of the medium.
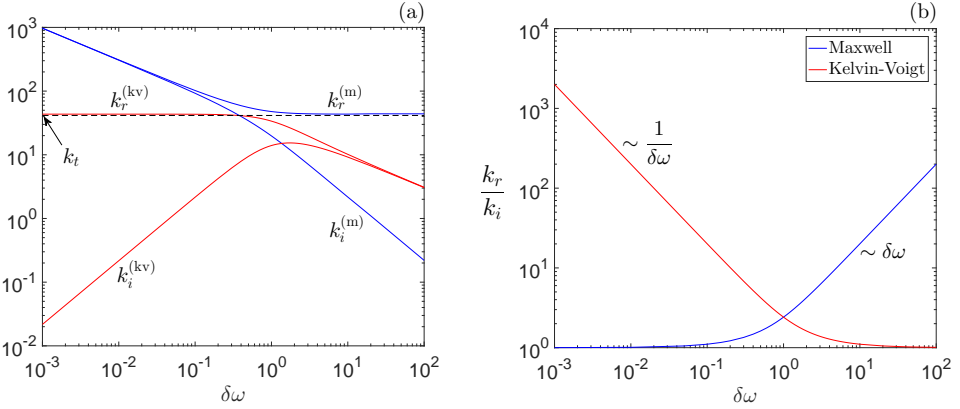
FIG. 2. Rayleigh wavenumber as a function of normalized frequency $\delta\omega$ for Maxwell and Kelvin–Voigt models. The superscript $^{(m)}$ is used throughout this article for the Maxwell model and the superscript $^{(kv)}$ is employed for the Kelvin–Voigt model.

3.2. Comparison of Zener, Maxwell and Kelvin–Voigt models

The Rayleigh wavenumber of Zener, Maxwell and Kelvin–Voigt models are compared in Fig. 3 and two cases can be distinguished. For $\alpha = 0$ the Zener model coincides with the Maxwell one. For $\alpha \neq 0$ the real part of the Rayleigh wavenumber for the Zener model keeps a constant value (first plateau) if $\delta\omega \leq 0.1$, declines and reaches a second plateau if $\delta\omega \geq 1$. Two elastic regions for $\delta\omega \leq 0.1$ and $\delta\omega \geq 1$ and one viscoelastic transition zone in between are pointed up for the Zener model. On the other hand, as the normalized frequency increases, the imaginary part of the Rayleigh wavenumber for the Zener model first increases, reaches a maximum and then decreases. To justify these analyses, the following asymptotic relations based on the first-order Taylor polynomial can be used:

$$
(3.3) \quad
\begin{aligned}
&k_r^{(z)} = \frac{k_t}{\sqrt{\alpha}}, \quad k_i^{(z)} = \frac{k_t \delta\omega}{\sqrt{2\alpha}} \quad \text{for } \delta\omega \ll 1, \\
&k_r^{(z)} = \frac{k_t}{\sqrt{\alpha+1}}, \quad k_i^{(z)} = \frac{k_t}{\sqrt{2}\delta\omega(\alpha+1)^{3/2}}, \quad \text{for } \delta\omega \gg 1,
\end{aligned}
$$

where the superscript $^{(z)}$ is used for the Zener model. Moreover, Fig. 3 highlights a very important result. As expected, the Zener model is analogous to
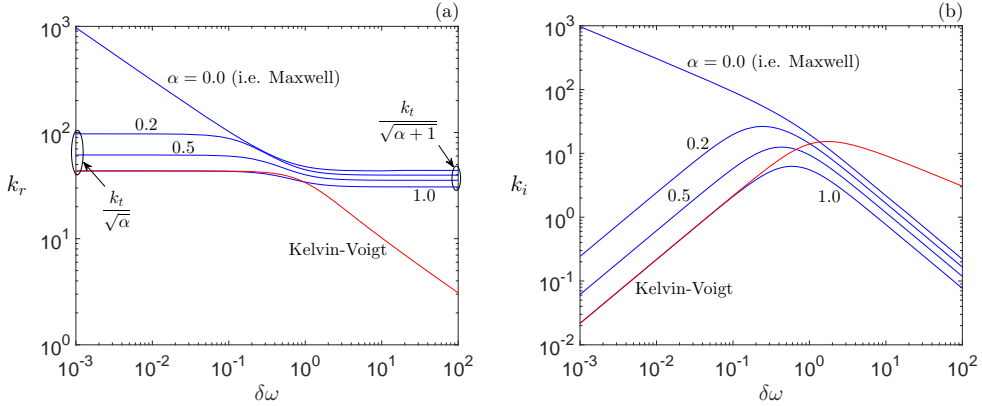
Fig. 3. Rayleigh wavenumber as a function of normalized frequency $\delta\omega$ for Zener, Maxwell and Kelvin–Voigt models for different values of $\alpha = G_2/G_1$.

the Kelvin–Voigt model for the low normalized frequency. While for the high normalized frequency the Zener model coincides with the Maxwell model.

3.3. Influence of the shear moduli ratio on the Rayleigh wave velocity and attenuation

The influence of the shear moduli ratio on the Rayleigh wave velocity and attenuation is illustrated in Figs. 4 and 5. Firstly, Fig. 4 supplies the evolution of the Rayleigh wave velocity and attenuation as a function of the normalized frequency for different values of shear modulus ratio α. For $\alpha = 0$, the velocity rises quickly for low $\delta\omega$ values and then reaches a plateau region (c_t). Otherwise, the attenuation decreases monotonically. If $\alpha \neq 0$, the velocity has a constant value ($\sqrt{\alpha}c_t$) for very low $\delta\omega$ values, increases and a constant value ($\sqrt{\alpha + 1}c_t$) is obtained for very high $\delta\omega$. In addition, for fixed value of $\delta\omega$, the velocity augments and the attenuation diminishes with α. It is noted that the behavior of the velocity observed here can be deduced from the real part of the wavenumber pointed up in Fig. 3 since the velocity is inversely proportional to this real part.

Secondly, the wave velocity and attenuation are plotted for six values of the normalized frequency $\delta\omega$ as a function of the shear modulus ratio α. The velocity keeps a constant value for $\alpha \leq 0.1$ then increases with α. For a well determined α value, the velocity grows with $\delta\omega$. For $\alpha \geq 0.1$, the influence of α on the velocity is less important. The six curves converge for $\alpha = 10$. In this last case the velocity does not depend on $\delta\omega$. Therefore, this behavior is typically elastic. This observation is in good agreement with the evolution of the attenuation given in Fig. 5(b). Furthermore, the attenuation decreases monotonically with α and converges to 0 for any value of $\delta\omega$. However, the attenuation curves converge faster when $\delta\omega$ is lower.
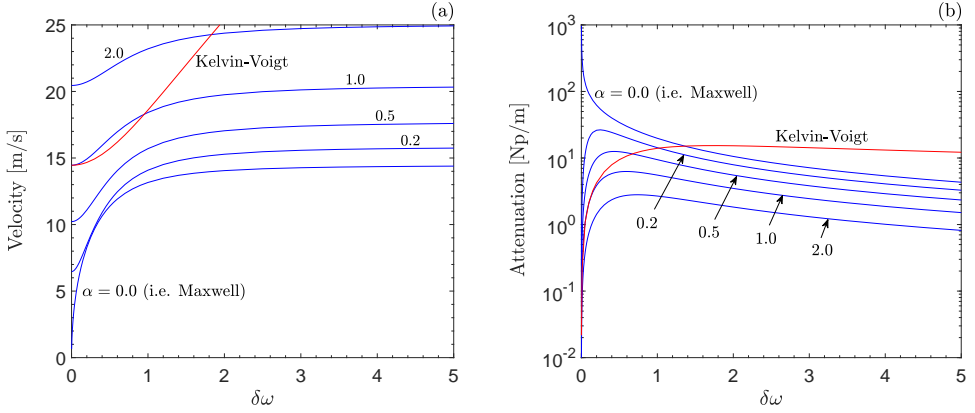
FIG. 4. Rayleigh wave velocity and attenuation versus normalized frequency $\delta\omega$ for different values of shear moduli ratio α.
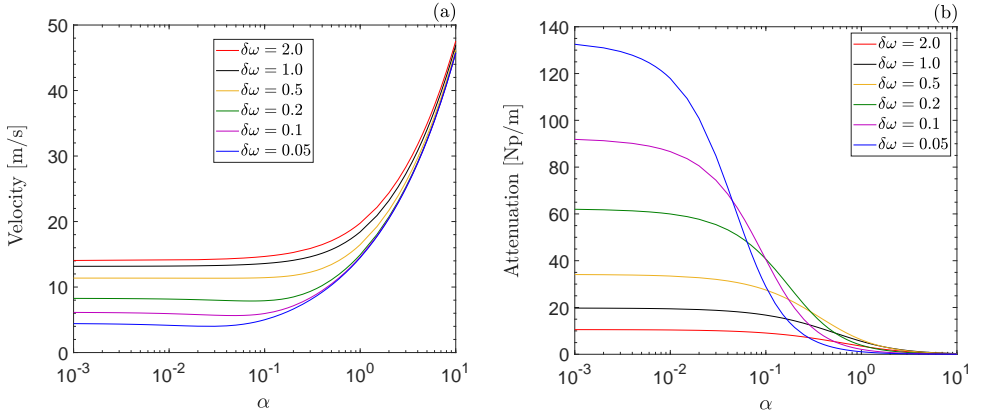
FIG. 5. Rayleigh wave velocity and attenuation versus shear moduli ratio α for different values of normalized frequency $\delta\omega$.

4. Validation of the present method

In this section, we compare the theoretical predictions of the dispersion equation to literature theoretical and experimental data collected from a previously published paper [3]. CATHELINE et al. presented an experimental device considering only shear wave. Therefore, the analytical model used by CATHELINE et al. is adapted to the experiment, i.e. considering a one-dimensional shear wave.

To plot the Rayleigh wave velocity and attenuation as a function of frequency for the Zener model, the experimental shear moduli given in [3] are used. In consequence, $G_1 = 5.73\,\text{kPa}$ and $\eta = 23\,\text{Pa}\cdot\text{s}$ for the Zener model with $\alpha = 0$. Otherwise, $G_1 = 5.67\,\text{kPa}$ and $\eta = 0.22\,\text{Pa}\cdot\text{s}$ if $\alpha = 1$. As observed in Fig. 6, the velocity and attenuation calculated for the Zener model with $\alpha = 0$ increases

with the frequency and reaches a plateau region for $f \gg 40\,\mathrm{Hz}$ ($\delta\omega \gg 1$). This is coherent with the asymptotic relations given in the following form:

$$v^{(\mathrm{m})} = c_t\sqrt{\delta\omega}, \quad k_i^{(\mathrm{m})} = \frac{\sqrt{\omega}}{c_t\sqrt{\delta}} \quad \text{for } f \ll 40\,\mathrm{Hz},$$

(4.1)

$$v^{(\mathrm{m})} = c_t, \quad k_i^{(\mathrm{m})} = \frac{1}{\sqrt{2}c_t\delta} \quad \text{for } f \gg 40\,\mathrm{Hz}.$$

Moreover, it is also shown (Fig. 6) that the velocity keeps a constant value for the Zener model with $\alpha = 1$ and frequency less than $500\,\mathrm{Hz}$. We can also notice that the attenuation increases monotonically with the frequency. This can be justified by the coincidence between Zener ($\alpha = 1$) and Kelvin–Voigt models (Fig. 3) for $\delta\omega \ll 1$ or $f \ll 4000\,\mathrm{Hz}$. Otherwise, these curves are asymptotically approaches by the two subsequent equations:

(4.2) $\qquad v^{(\mathrm{kv})} = c_t\sqrt{\delta\omega}, \quad k_i^{(\mathrm{kv})} = \frac{\delta\omega^2}{\sqrt{2}c_t} \quad \text{for } \delta\omega \ll 1 \text{ or } f \ll 4000\,\mathrm{Hz}.$

Finally, the theoretical curves in Fig. 6 are in very good agreement with those obtained by Catheline *et al.* [3].
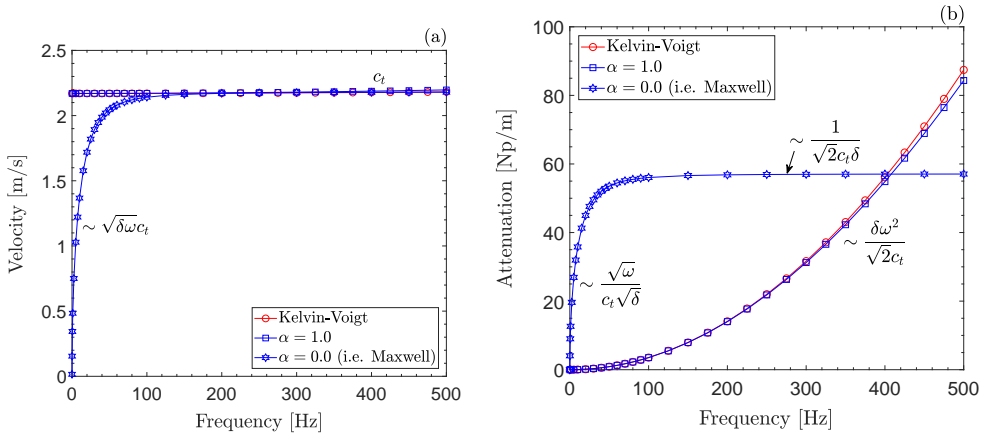
Fig. 6. Rayleigh wave velocity and attenuation versus frequency for Maxwell and Kelvin–Voigt models.

5. Particular configuration of the standard linear solid model

As mentioned previously, the model that captures both the relaxation and retardation is known as the three-parameter model or the standard linear solid (SLS) model. Another configuration of the SLS model is obtained by adding a spring in series to the Kelvin–Voigt model. This model is sometimes referred

to as the Poynting–Thomson model. A comparison between Poynting–Thomson and Zener models is made in this section. It is therefore necessary to establish the constitutive equation characterizing the Poynting–Thomson model. This constitutive equation can be obtained using equilibrium and compatibility conditions as follow:

$$(G_1 + G_2)\boldsymbol{\tau} + \eta\frac{\partial\boldsymbol{\tau}}{\partial t} = 2G_1 G_2\boldsymbol{\varepsilon} + 2G_1\eta\frac{\partial\boldsymbol{\varepsilon}}{\partial t}.$$

In this case the generalized unsteady momentum Eq. (2.3) becomes:

$$\frac{\rho}{G_1}\left[(1+\alpha)\frac{\partial^2\mathbf{u}}{\partial t^2} + \delta\frac{\partial^3\mathbf{u}}{\partial t^3}\right] = \left[\frac{\lambda}{G_1} + \alpha\left(1+\frac{\lambda}{G_1}\right) + \delta\left(1+\frac{\lambda}{G_1}\right)\frac{\partial}{\partial t}\right]\nabla\nabla\cdot\mathbf{u}$$
$$+ \left(\alpha + \delta\frac{\partial}{\partial t}\right)\nabla^2\mathbf{u}.$$

For harmonic behavior, the complex elastic modulus given in Eq. (1.2) can be expressed as:

$$(5.1) \qquad\qquad \frac{G(\omega)}{G_1} = \frac{\alpha - j\omega\delta}{1 + \alpha - j\omega\delta}.$$

Note that the dispersion equation in the case of the Poynting–Thomson model is similar to dispersion equation (2.18). To plot the Rayleigh wave properties, the complex shear modulus (Eq. (5.1)) is introduced into the dispersion equation (2.18). Figure 7 shows the influence of the model used on the Rayleigh wave velocity and attenuation. Velocity and attenuation are plotted against the normalized frequency $\delta\omega$ for the two SLS configurations. In this figure, velocity and attenuation have been plotted over a wide range of variation of the normalized
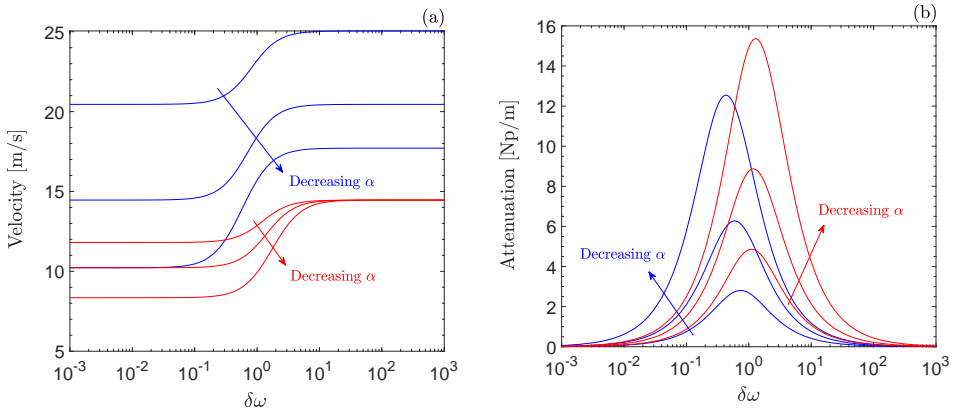
FIG. 7. Rayleigh wave properties versus normalized frequency $\delta\omega$ for three values of moduli ratio $\alpha = 0.5, 1, 2$. Blue lines represent zener model and red lines for the Poynting–Thomson model.

frequency $\delta\omega$, and for three values of the shear modulus ratio. The attenuation behavior in the case of the Poynting–Thomson model is similar to that of the Zener model. However, the amplitude and positions of local maxima are different. For the Rayleigh wave velocity, the difference between the two models is linked to the modulus ratio effect on the second plateau corresponding to the second elastic zone.

6. Conclusion

Propagation of Rayleigh waves in a viscoelastic media was investigated in this paper using an original approach based on the exact theory. A new theoretical form of the complex dispersion equation was developed. The effect of the normalized frequency $\delta\omega$ on the Rayleigh wave number was investigated for Maxwell, Kelvin–Voigt and Zener models. The influence of the shear modulus ratio (Zener model) on the Rayleigh wave velocity and attenuation was also studied. The comparison between Zener, Maxwell and Kelvin–Voigt models points up a very important result. As expected, one can conclude that the behavior of the Zener model is analogous to the Kelvin–Voigt model (Creep) for the low normalized frequency and to the Maxwell model (relaxation) for the high normalized frequency. Consequently, the Zener model can be used to describe the creep behavior (as the Kelvin–Voigt model) and the relaxation behavior (as the Maxwell model).

Conflict of interest

The authors declare that they have no conflict of interest.

References

1. C. Villa, M.A.J. Chaplain, A. Gerisch, T. Lorenzi, *Mechanical models of pattern and form in biological tissues: the role of stress-strain constitutive equations*, Bulletin of Mathematical Biology, **83**, 80, 2021.

2. S.S. Poul, J. Ormachea, G.R. Ge, K.J. Parker, *Comprehensive experimental assessments of rheological models performance in elastography of soft tissues*, Acta Biomaterialia, **146**, 259–273, 2022.

3. S. Catheline, J.L. Gennisson, G. Delon, M. Fink, R. Sinkus, S. Abouelkaram, J. Culioli, *Measuring of viscoelastic properties of homogeneous soft solid using transient elastography: an inverse problem approach*, The Journal of the Acoustical Society of America, **116**, 3734, 2004.

4. A.P. Saravazyan, M.W. Urban, J.F. Greenleaf, *Acoustic waves in medical imaging and diagnostics*, Ultrasound in Medicine and Biology, **39**, 1133–1146, 2013.

5. S. Kazemirad, *Wave propagation for the experimental characterization of soft biomaterials and tissues*, PhD Thesis, McGill University, 2014.

6. S. Kazemirad, H.K. Heris, L. Mongeau, *Experimental methods for the characterization of the frequency-dependent viscoelastic properties of soft materials*, The Journal of the Acoustical Society of America, **133**, 3186–3197, 2013.

7. S. Kazemirad, L. Mongeau, *Rayleigh wave propagation method for the characterization of a thin layer of biomaterials*, The Journal of the Acoustical Society of America, **133**, 4332–4342, 2013.

8. J.D. Ferry, *Viscoelastic Properties of Polymers*, 3rd ed., Wiley & Sons, 1980.

9. R.G. Larson, *The structure and rheology of complex fluids*, Oxford University Press, 1999.

10. J.D. Achenbach, C.C. Chao, *A three-parameter viscoelastic model particularly suited for dynamic problems*, Journal of the Mechanics and Physics of Solids, **10**, 245–252, 1962.

11. S. Alonso, M. Radszuweit, H. Engel, M. Bar, *Mechanochemical pattern formation in simple models of active viscoelastic fluids and solids*, Journal of Physics D: Applied Physics, **50**, 434004, 2017.

12. K. J. Parker, T. Szabo, S. Holm, *Towards a consensus on rheological models for elastography in soft tissues*, Physics in Medecine and Biology, **64**, 215012, 2019.

13. J. F. Greenleaf, M. Fatemi, M. Insana, *Selected methods for imaging elastic properties of biological tissues*, Annual Review of Biomedical Engineering, **5**, 57–78, 2003.

14. A.P. Sarvazyan, O.V. Rudenko, S.D. Swanson, J.B. Fowlkes, S.Y. Emelianov, *Shear wave elasticity imaging: A new ultrasonic technology of medical diagnostics*, Ultrasound in Medicine and Biology, **24**, 1419–1435, 1998.

15. S. Kazemirad, S. Bernard, S. Hybois, A. Tang, G. Cloutier, *Ultrasound shear wave viscoelastography: model-independent quantification of the complex shear modulus*, IEEE Transactions on Ultrasonics, Ferroelectrics, and Frequency Control, **63**, 1399–1408, 2016.

16. S. Chen, M. Fatemi, J.F. Greenleaf, *Quantifying elasticity and viscosity from measurement of shear wave speed dispersion*, The Journal of the Acoustical Society of America, **115**, 2781, 2004.

17. S. Chen, M.W. Urban, C. Pislaru, R. Kinnick, Y. Zheng, A. Yao, J.F. Greenleaf, *Shearwave dispersion ultrasound vibrometry (SDUV) for measuring tissue elasticity and viscosity*, IEEE Trans Ultrason Ferroelectr Freq Control, **56**, 55–62, 2009.

18. I.Z. Nenadic, M.W. Urban, S. Aristizabal, S.A. Mitchell, T.C. Humphrey, J.F. Greenleaf, *On Lamb and Rayleigh wave convergence in viscoelastic tissues*, Physics in Medicine & Biology, **56**, 6723–6738, 2011.

19. I.Z. Nenadic, M.W. Urban, S.A. Mitchell, J.F. Greenleaf, *Lamb wave dispersion ultrasound vibrometry (LDUV) for quanification of mechanicao properties of viscoelastic solids*, Physics in Medecine and Biology, **56**, 2245–2264, 2011.

20. R.W.S. Chan, I.R. Titze, *Viscosities of implantable biomaterials in vocal fold augmentation surgery*, Laringoscope, **108**, 725–731, 1998.

21. R.W.S. Chan, I.R. Titze, *Hyaluronic acid (with fibronectin) as a bioimplant for the vocal fold mucosa*, Laringoscope, **109**, 1142–1149, 1999.

22. R.W.S. Chan, M.L. Rodrigez, *A simple-shear rheometer for linear viscoelastic characterization of vocal fold tissues at phonatory frequencies*, The Journal of Acoustical Society of America, **124**, 4332–4342, 1998.

23. I.R. Titze, S.A. Klemuk, S. Gray, *Methodology for rheological testing of engineered biomaterials at low audio frequencies*, The Journal of Acoustical Society of America, **115**, 392–401, 2004.

24. J.L. Vanderhooft, M. Alcoutlabi, J.J. Magda, G.D. Prestwich, *Rheological properties of cross-linked hyaluronan-gelatin hydrogels for tissue engineering*, Macromolecular Bioscience, **9**, 20–28, 2009.

25. J.D. Achenbach, *Wave Propagation in Elastic Solids*, North-Holland, Amsterdam, 1973.

26. E. Dieulesaint, D. Royer, *Ondes élastiques dans les solides*, Masson, Paris, 1974.

27. B.A. Auld, *Acoustic fields and waves in solids*, 1990.

28. L. Landau, E. Lifchitz, *Théorie de l'élasticité*, Mir, Moscou, 1990.

29. I. Kaur, P. Lata, *Rayleigh wave propagation in transversely isotropic magneto-thermoelastic medium with three-phase-lag heat transfer and diffusion*, International Journal of Mechanical and Materials Engineering, **14**, 12, 2019.

30. P. Lata, Himanshi, *Rotational and fractional effect on Rayleigh waves in an orthotropic magneto-thermoelastic media with hall current*, Steel and Composite Structures, **42**, 723–732, 2022.

31. P. Lata, S. Singh, *Rayleigh wave propagation in a nonlocal isotropic magneto-thermoelastic solid with multi-dual-phase lag heat transfer*, GEM – International Journal on Geomathematics, **13**, 5, 2022.

32. C. Pecorari, *Modeling variations of Rayleigh wave velocity due to distributions of one-dimensional surface-breaking cracks*, The Journal of the Acoustical Society of America, **100**, 1452–1550, 1996.

33. C. Pecorari, *Attenuation and dispersion of Rayleigh waves propagating on a cracked surface: an effective field approach*, Ultrasons, **38**, 754–760, 2000.

34. M.D. Sharma, *Rayleigh wave at the surface of a general anisotropic poroelastic medium: derivation of real secular equation*, Proceedings of the Royal Society A, **474**, 20170589, 2018.

35. K. Aki, P. Richards, *Quantitative Seismology, Theory and Methods*, Freeman, San Francisco, 1980.

36. K.S. Beaty, D.R. Schmitt, M. Sacchi, *Simulated annealing inversion of multimode Rayleigh wave dispersion curves for geological structure*, Geophysical Journal International, **151**, 622–631, 2002.

37. J. Xia, E. Nyquist, Y. Xu, M.J.S. Roth, R.D. Miller, *Feasibility of detecting near-surface feature with Rayleigh-wave diffraction*, Journal of Applied Geophysics, **62**, 244–253, 2007.

38. J. Xia, R.D. Miller, C.B. Park, *Estimation of near-surface shear-wave velocity by inversion of Rayleigh wave*, Geophysics, **64**, 691–700, 1999.

39. X.H. Campman, K. van Wijk, C.D. Riyanti, J. Scales, G.C. Herman, *Imaging scattered seismic surface waves*, Near Surface Geophysics, **2**, 223–230, 2004.

40. P.K. Currie, M.A. Hayes, P.M. O'Leary, *Viscoelastic Rayleigh waves*, Quarterly of Applied Mathematics, **35**, 35–53, 1977.

41. P.K. Currie, P.M. O'Leary, *Viscoelastic Rayleigh waves II*, Quarterly of Applied Mathematics, **35**, 445–454, 1978.

42. P.K. Currie, *Viscoelastic surface waves on a standard linear solid*, Quarterly of Applied Mathematics, **37**, 332–336, 1979.

43. J.M. Carcione, *Rayleigh waves in isotropic viscoelastic media*, Geophysical Journal International, **108**, 453–464, 1992.

44. T.J. Royston, H.A. Mansy, R.H. Sandler, *Excitation and propagation of surface waves on a viscoelastic half-space with application to medical diagnosis*, The Journal of the Acoustical Society of America, **106**, 3678–3686, 1999.

45. T.J. Royston, Z. Dai, R. Chaunsali, Y. Liu, Y. Peng, R.L. Magin, *Estimating material viscoelastic properties based on surface wave measurements: a comparison of techniques and modeling assumptions*, The Journal of the Acoustical Society of America, **130**, 4126–4138, 2011.

46. T. Alfrey, *Mechanical Behavior of High Polymers*, Interscience, New York, 1948.

47. E.J. Scott, *Wave propagation in a visco-elastic medium*, Quarterly of Applied Mathematics, **12**, 300–306, 1954.

48. T. Alfrey, *Mechanical Behavior of High Polymers – Overview and Historic Remarks*, Springer, Boston, 1973.

49. A.F. Bower, *Applied Mechanics of Solids*, CRC Press, 2009.

50. P.M. Morse, H. Feshbach, *Methods of Theoretical Physics, Part II*, McGraw-Hill, New York, 1946.